Interstitial Lung Diseases

26

Christina Mueller-Mang, Christina Plank, Helmut Ringl, Albert Dirisamer and Christian Herold

CONTENTS

ABSTRACT

The term interstitial lung disease (ILD) comprises a diverse group of diseases that lead to *inflammation* and *fibrosis* of the alveoli, distal airways, and septal interstitium of the lungs. The ILDs consist of disorders of *known cause* (e.g., collagen vascular diseases, drug-related diseases) as well as disorders of unknown etiology. The latter include *idiopathic interstitial pneumonias* (IIPs), sarcoidosis and a group of miscellaneous, rare, but nonetheless interesting, diseases. In patients with ILD, MDCT enriches the diagnostic armamentarium by allowing volumetric high resolution scanning, i.e., continuous data acquisition with thin collimation and a high spatial frequency reconstruction algorithm. *CT* is a key method in the identification and man-

C. Mueller-Mang, MD
Department of Radiology, Medical University of Vienna, Waehringer Guertel 18–20, 1190 Vienna, Austria

C. Plank, MD
Department of Radiology, Medical University of Vienna, Waehringer Guertel 18–20, 1190 Vienna, Austria

H. Ringl, MD
Department of Radiology, Medical University of Vienna, Waehringer Guertel 18–20, 1190 Vienna, Austria

A. Dirisamer, MD
Department of Radiology, Medical University of Vienna, Waehringer Guertel 18–20, 1190 Vienna, Austria

C. Herold, MD
Department of Radiology, Medical University of Vienna, Waehringer Guertel 18–20, 1190 Vienna, Austria

agement of patients with ILD. It not only improves the detection and characterization of parenchymal abnormalities, but also increases the accuracy of diagnosis. The spectrum of morphologic characteristics that are indicative of interstitial lung disease is relatively limited and includes a reticular pattern (with or without traction bronchiectasis), thickening of interlobular septa, honeycombing, nodules, and ground-glass opacities. In the correct clinical context, some *patterns* or combination of patterns, together with the *anatomic distribution* of the abnormality, i.e., from the lung apex to the base, or peripheral subpleural versus central bronchovascular, can lead the interpreter to a specific diagnosis. However, due to an overlap of the CT morphology between the various entities, complementary *lung biopsy* is recommended in virtually all cases of ILDs.

26.1 Introduction

The interstitial lung diseases (ILDs) are a heterogeneous group of lung disorders that result from damage to the lung by various forms of inflammation and fibrosis. By definition, ILDs involve the lung interstitium that forms a fibrous skeleton for the lungs. However, many of the conditions that have been traditionally included under the heading of ILDs are actually associated with extensive alterations of the alveolar and airway architecture. For this reason, the terms *diffuse infiltrative lung disease* or *diffuse parenchymal lung disease* are preferable. Still, the term ILDs remains in common clinical usage.

ILDs represent more than 200 different entities, and various and often-confusing classification systems are simultaneously used. One useful approach to classification is to separate the ILDs into diseases of known and

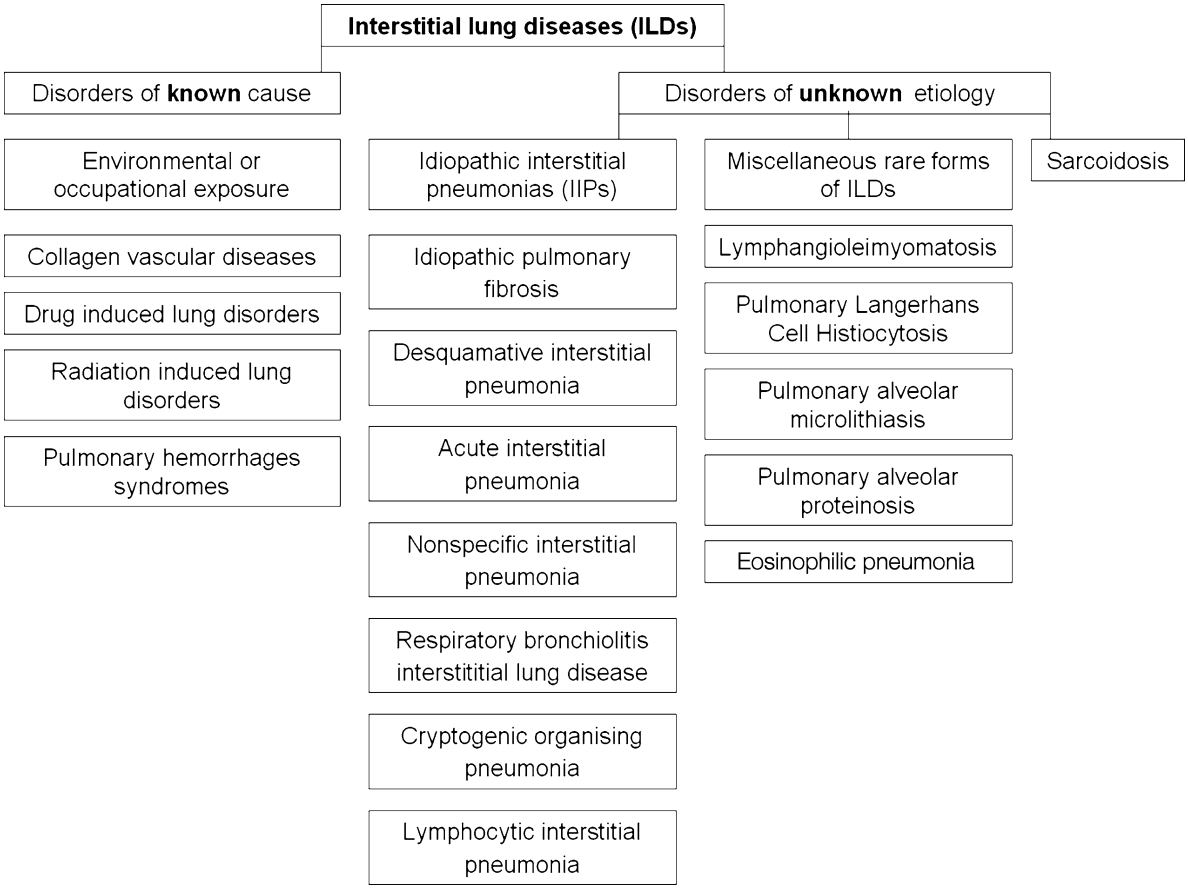

Fig. 26.1 Classification of interstitial lung diseases (*ILDs*)

unknown etiology (Fig. 26.1). ILD of unknown etiology (65% of all ILDs) can be further subdivided into the group of idiopathic interstitial pneumonias (IIPs), and a group comprising several rare but interesting diseases with distinctive clinicopathologic features, such as lymphangioleiomyomatosis, Langerhans cell histiocytosis, pulmonary alveolar proteinosis, and pulmonary alveolar microlithiasis. Sarcoidosis has an exceptional position within the group of ILDs of unknown cause, as it is relatively common and can present as a systemic disease.

CT scanning is the most important noninvasive diagnostic key to the identification and characterization of ILD, and aids the radiologist and the clinician in the management of patients who carry this disorder. Among all noninvasive methods, it provides the highest sensitivity and specificity in the detection of ILD. Also, it has a higher accuracy in comparison to the clinical assessment, lung function tests, and chest radiography in diagnosing a specific disorder, and adds diagnostic accuracy and confidence when added to the clinical assessment and the chest radiogram. Finally, CT helps to identify the best location for lung biopsy, and provides an important basis for the follow-up of ILD patients.

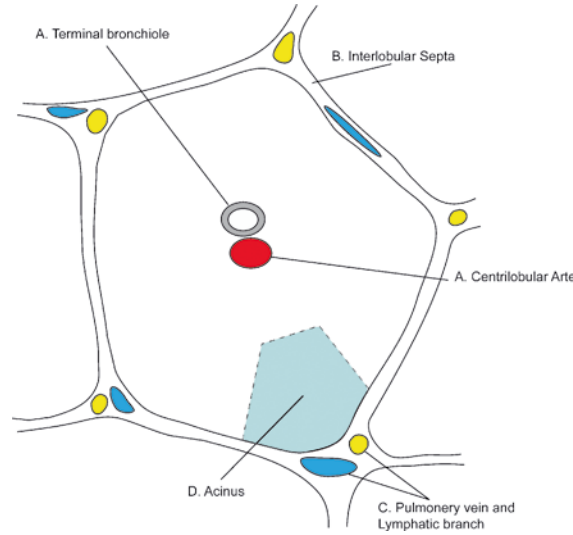

Fig. 26.2. Secondary pulmonary lobule (*A* centrilobular arteries and bronchioles with a diameter of approximately 1 mm, *B* interlobular septa with a thickness of approximately 0.1 mm, *C* pulmonary vein and lymphatic branch with diameters of 0.5 mm each, *D* acinus—never visible on CT scans)

26.2 Anatomic and Technical Considerations

26.2.1 Normal Lung Anatomy

The correct interpretation of CT and especially high-resolution CT (HRCT) requires a fundamental understanding of normal lung anatomy. In patients with ILD, the small anatomical structures of the lung parenchyma such as the secondary pulmonary lobule are involved in one way or another, and the identification of the patterns of infiltration and distribution is a key to the establishment of a correct list of differential diagnoses, and sometimes to the diagnosis itself. In this sense, HRCT provides an insight into lung morphology and architecture, comparable to or even beyond macroscopic pathology. The following anatomic structures and architectural components need to be considered:

The Secondary Pulmonary Lobule

The secondary pulmonary lobule is the smallest anatomical unit of the lungs that can be identified on high-resolution CT scans (Fig. 26.2). Whereas in normal lungs, these polyhedral structures are only visible in the anterior and lateral portions of the pulmonary parenchyma, they may be identifiable in any region when ILD and other disorders such as lung edema are present.

Typical secondary pulmonary lobules are irregular polyhedral units that vary in size, measuring from approximately 1 to 2.5 cm in diameter and incorporating up to 24 acini (Webb 2006). An average diameter for pulmonary lobules ranges from 11 to 17 mm in adults. The secondary pulmonary lobule is surrounded by a mantle of connective tissue septa. A central bronchovascular bundle, consisting of the lobular bronchiole and the accompanying pulmonary artery, enters the center of the secondary pulmonary lobule, where the bronchiole bifurcates into three to five terminal bronchioles. The region near the origin of the terminal bronchioles is termed the "centrilobular" region. Thus, on thin-section CT images, the secondary pulmonary lobule can be divided into three components: the interlobular septa, the centrilobular region, and the lobular parenchyma.

Interlobular Septa

The interlobular septa extend from the pleural surface of the lung inward, and surround the secondary lobule. They consist of connective tissue, house pulmonary veins, and lymphatics and belong to the peripheral in-

terstitial fiber system (Weibel 1979). Interlobular septa are well developed in the periphery of the lungs, and in particular in the lung apex, and near the anterior, lower, mediastinal, and diaphragmatic surfaces. They are key structures to the identification of pulmonary involvement in ILD, because disorders such as interstitial pneumonia, sarcoidosis or lymphangitic carcinomatosis commonly lead to thickening and consequently, to better visibility of these structures.

Centrilobular Region

The centrilobular region corresponds to the "axial fiber system" described by Weibel (1979). The central portion of the secondary pulmonary lobule contains the pulmonary artery and bronchiolar branches that supply the lobule. Because lobules do not arise at a specific branching generation of the bronchial or arterial tree, it is difficult to impossible to define exactly which specific bronchus or artery supplies that secondary lobule. However, lobular bronchioles are rarely seen in normal individuals since their lumen measures approximately 1 mm in diameter, and their wall 0.15 mm, respectively. Likewise, the more peripheral terminal and respiratory bronchioles cannot be resolved at CT (Murata et al. 1986). It is only in diseases of the small airways that abnormal bronchi can be visualized through thickened walls, peribronchiolar inflammation, and/or intrabronchiolar fluid and mucus accumulations. Centrilobular arteries can be depicted on CT scans of normal and diseased individuals. Because of the anatomic properties of the lungs, centrilobular abnormalities are best seen in the lung periphery and near the hila.

Lobular Parenchyma

The lung (lobular) parenchyma consists of alveoli, connective tissue, and the associated pulmonary capillary bed. These structures are too small to be directly visualized on thin-section CT, but may be indirectly assessed, as they are responsible for the background density of the lung on CT scans. Parenchymal background density reflects the proportions of fluid (blood and extravascular fluid), gas, and tissue. When ILD causes an increase of fluid or cells within the alveoli, or thickening of the alveolar septa through cellular infiltration or fibrosis, then parenchymal background density will change in turn and ground glass opacities may be identified at CT. Conversely, a decrease in fluid, cells, and tissue (in relation to air), as seen in emphysema, causes a reduction of the parenchymal density, in comparison to the normal state.

26.2.2 CT Technique

For patients with ILD, the identification of the smallest possible structures of the lung parenchyma and the depiction of their abnormalities is of paramount importance for any imaging approach. Therefore, CT protocols have to utilize thin collimation and high-spatial-frequency reconstruction algorithms to achieve an optimal spatial resolution and consequently, facilitate an optimal assessment of interstitial and airspace disease. For decades, patients with ILD have traditionally been investigated with HRCT (Mayo et al. 1987). This technique consists of a "step-and-shoot" approach, in which 0.5- to 1-mm collimation scans are obtained at 10- to 20-mm intervals, a small FOV, and a high radiation dose per section. It provides excellent image quality, free of partial volume and projection artifacts, and combines high sensitivity in the detection of ILD with high accuracy in establishing the correct diagnosis. This "classic" HRCT technique still plays a decisive role in the noninvasive investigation of patients with pulmonary disease of a diffuse distribution pattern (Hansell 2001).

With the advent of MDCT, volumetric high-resolution imaging has enriched the diagnostic armamentarium of the radiologist. New-generation MDCT scanners allow fast single-breath-hold scanning, volumetric data acquisition with thinly collimated scans, and high-spatial-frequency reconstruction when scanning the entire lung. They thus combine the advantages of "traditional" HRCT and modern spiral scanning techniques. Volumetric protocols enable the radiologist to detect those abnormalities that might have been missed during the classic HRCT step-and-shoot approach. Moreover, volumetric isotropic data sets permit the reconstruction of high-quality multiplanar images, which help to appreciate better the distribution of disease, for example, to identify a cephalocaudal gradient of disease severity in certain disorders. Finally, continuous data acquisition allows the generation of MIP images, which in our experience, are helpful in the detection of micronodular disease and centrilobular abnormalities.

There are also some trade-offs with volumetric HRCT scanning. The radiation dose is 5 to 10 times higher, and the image quality is discretely lower in comparison to classic sequential HRCT. This image quality reduction is most apparent in the depiction of small septa and of ground-glass opacities (Studler et al. 2005) (Fig. 26.3a,b), and its clinical significance has yet to be determined. In order to achieve the best possible balance between diagnostic accuracy, exploitation of the advantages of volumetric CT and radiation dose, the following options exist (Table 26.1):

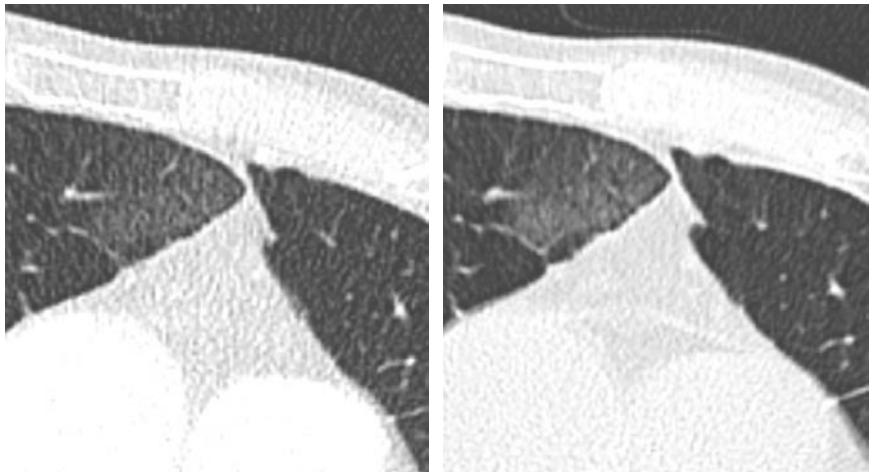

Fig. 26.3a,b. Difference in ground-glass depiction between sequential HRCT (**a**) and standard helical CT with 1-mm section thickness (**b**)

1. Sequential HRCT protocol
   This protocol utilizes high milliampere-second and kilovolt peak values to obtain the best possible image quality. Thin collimation (1 mm) scans are obtained at 10- or 20-mm intervals. Therefore, the overall radiation dose is a 5th to a 10th in comparison to standard or high-resolution volumetric protocols. This protocol may be regarded as "imaging biopsy" in diffuse lung disease, as it detects disease, allows the specification of disease distribution, and helps in establishing a differential diagnosis with high accuracy and confidence levels. It is our protocol of choice in patients with proven ILD, and in those cases that require imaging follow-up during or after therapy. Because the classic HRCT leaves 9- to 19-mm broad gaps between the scanned sections unexamined, it should not be utilized as sole protocol in patients with suspicion of focal lung disease, in diffuse interstitial disorders where there is an increased risk associated with focal or even malignant abnormalities (such as dermatomyositis/polymyositis), or in entities with a distinct propensity to involve extrapulmonary sites in the mediastinum, the chest wall, the diaphragm, and the abdomen. In such instances, a combination with a standard volumetric protocol (Table 26.1) is highly

Table 26.1. Various MDCT protocols of the lung, valid for the Siemens Somatom Sensation 64 Cardiac scanner

Protocol	Kilovolt peak	Current reference mAs/actual mAs	Dose modulation	Collimation (mm × slice no.)	Section thickness/reconstruction slice interval (mm/mm)	Dose length product (mGy × cm)	Effective dose (mSv)
HRCT sequential	140	200/200	Off	1 × 2	1/20	60	1
HRCT volumetric	140	240/240	Off	0.6 × 64	1/0.8	800	13
Standard volumetric	120	200/80–120	On	0.6 × 64	1/0.8	300	5.1
Low-dose volumetric	80	30/30	Off	0.6 × 64	3/5	40	0.68

The reference mAs is the current preset of the protocol; the scanner controls the actual mAs within certain limits of this reference according its dose-modulation program

recommended. Another caveat is the assessment of patients with suspected air trapping at supine scans. In these cases, it is advisable to perform single slice step-and-shoot scans in prone positions instead of a continuous volumetric examination in order to reduce radiation burden.

2. Volumetric HRCT protocol
This protocol combines thin collimation with volumetric scanning and high milliampere-second and kilovolt peak values. During scanning, the dose modulation is off. The result is a high quality contiguous data set, which allows for high-resolution multiplanar and three-dimensional reconstructions with superb image quality. The latter is similar to that of sequential HRCT scanning, although it does not match it in every detail. The major disadvantage of this protocol is the radiation dose, which is approximately 10 times higher than that of conventional HRCT. We recommend using this protocol in ILD patients only when high-quality three-dimensional reconstructions are necessary, for example, for generating a data set for CT bronchoscopy.
3. Volumetric standard CT protocol
Here, the milliampere-second and kilovolt peak values are reduced in comparison to the sequential or volumetric high-resolution protocol, and dose modulation is switched on. The result is a substantial reduction in dose in comparison to the volumetric high-resolution protocol. Nevertheless, thin collimation and high-spatial-resolution reconstruction guarantee very good image quality, and volumetric data acquisition a continuous morphologic assessment of the lung investigated, respectively. In our view, this protocol is best used in combination with the classic sequential HRCT protocol in ILD patients. It provides a volumetric data set and the best high-resolution images, with a reasonable radiation dose that reaches roughly 50% of the dose resulting from the volumetric high-resolution protocol. It is advisable to utilize this combination protocol in all patients with ILD who are imaged for their first time, in cases where the chest radiogram indicates diffuse and focal disease, and in those who are at risk to develop focal disorders on top of a diffuse lung disease process.
4. Volumetric low-dose CT protocol
In patients with ILD, the low-dose high-resolution CT technique with a reduction of the milliampere-second values to approximately 40 mAs is in our view a valuable alternative to the standard volumetric protocol when combined with the sequential HRCT technique. It allows for the assessment of the pulmonary parenchyma in slim individuals, visualization of focal abnormalities in the lung parenchyma, and analysis of major airways disorders. The combination with the classic HRCT approach fosters almost the same advantages as those described for the combination of the standard volumetric protocol with classic HRCT. When using this protocol, one has to keep in mind that the somewhat reduced image quality may limit the diagnostic accuracy when scanning the parenchyma, the mediastinum, chest wall, and upper abdomen in obese patients.

26.3 Interstitial Lung Diseases That Have No Known Cause

In the majority of ILDs, the etiology remains either largely or wholly unknown. Most are uncommon, and some, such as alveolar microlithiasis, are exceedingly rare, but others, such as idiopathic pulmonary fibrosis and sarcoidosis, are quite common.

26.3.1 Idiopathic Interstitial Pneumonias

The term *idiopathic interstitial pneumonias* refers to a group of seven entities with distinct histologic patterns: idiopathic pulmonary fibrosis (IPF), characterized by the pattern of usual interstitial pneumonia (UIP); nonspecific interstitial pneumonia (NSIP); cryptogenic organizing pneumonia (COP); respiratory bronchiolitis-associated interstitial lung disease (RB-ILD); desquamative interstitial pneumonia (DIP); lymphoid interstitial pneumonia (LIP); and acute interstitial pneumonia (AIP).

In their idiopathic form, IIPs are rare diseases. They are, nevertheless, considered prototypes of more common secondary interstitial lung disorders, such as sarcoidosis, vasculitis, and connective tissue diseases, although they appear to follow a different and often less aggressive clinical course. The advent of HRCT has had a profound impact on the imaging of IIPs, because the detailed delineation of the lung anatomy allows a close correlation between the histologic patterns of IIPs and the CT features. On the basis of CT morphology and in the correct clinical context, the radiologist can achieve an accurate diagnosis in many cases. However, due to overlap between the various entities, complementary lung biopsy is recommended in virtually all cases.

26.3.1.1 Idiopathic Pulmonary Fibrosis

IPF is by far the most common IIP, and has a substantially poorer long-term survival rate than do the other IIPs (median survival rate is 2.5–3.5years) (Katzenstein and Myers 1998). IPF shares nonspecific clinical symptoms, such as gradual onset of progressive dyspnea and cough, with other IIPs. There is a slight male predominance, and patients are usually over the age of 50. Typically, patients do not respond to corticosteroid treatment, and currently, the only life-prolonging therapy consists of lung transplantation (Thabut et al. 2003). While the term IPF characterizes the clinical entity, the term *usual interstitial pneumonia* is used to describe the histologic and radiologic patterns associated with IPF. The histologic and radiologic features of UIP are characterized by heterogeneity with areas of normal lung alternating with patchy fibrosis. The typical CT findings in UIP are predominantly basal and peripheral reticular opacities with honeycombing and traction bronchiectasis (Fig. 26.4a) (Mueller-Mang et al. 2007). Ground-glass opacities are usually present, but limited in extent. However, in patients with rapid deterioration during the course of their illness, also referred to as acute exacerbation, widespread diffuse or patchy ground-glass opacities have been observed (Fig. 26.4b) (Kim et al. 2006). Other complications that should be noted in patients with IPF include opportunistic pulmonary infections (e.g., *Pneumocystis jiroveci*) and an increased risk of bronchial carcinoma (Bouros et al. 2002). Therefore, CT scanning should involve a combination of standard volumetric CT with sequential HRCT at regular intervals.

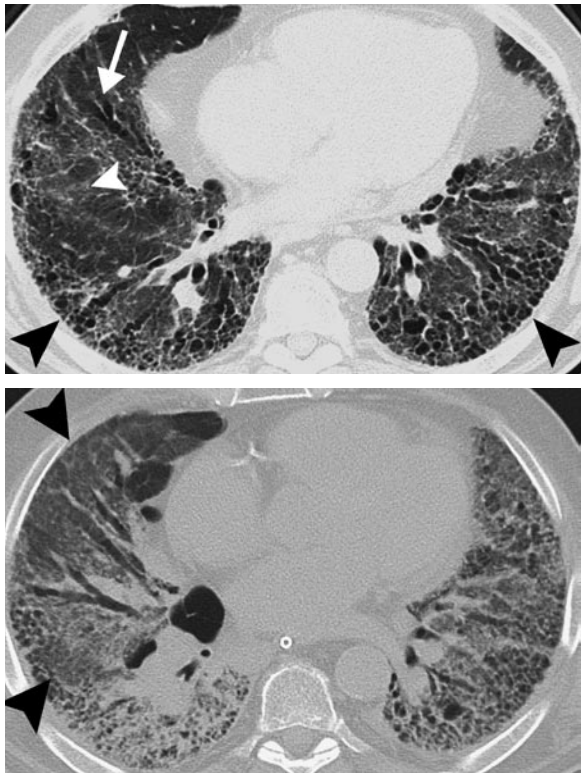

Fig. 26.4a,b. Axial CT image in a 63-year-old man with usual interstitial pneumonia (UIP)/idiopathic pulmonary fibrosis (IPF) shows bilateral reticular opacities, honeycombing (*black arrowheads*), and traction bronchiectasis (*arrow*). In addition, patchy, ground-glass opacities are present (*white arrowhead*) (**a**). Acute exacerbation in the same patient shows marked progression of ground-glass opacities (*arrowheads*) (**b**)

26.3.1.2 Nonspecific Interstitial Pneumonia

Given the clinical, radiologic, and pathologic variability of NSIP, the diagnostic approach to this entity is highly challenging, and the final diagnosis can be achieved only through interdisciplinary consensus. Patients with NSIP are usually between 40 and 50 years old, and men and women are equally affected. Compared with IPF, patients with NSIP have a variable, but overall more favorable, course of disease, and the majority of patients stabilizes or improves on corticosteroid therapy. According to the predominance of either inflammatory cells or fibrosis, NSIP is histologically subdivided into a cellular and a fibrotic subtype. Cellular NSIP is less common than is fibrotic NSIP and carries a substantially better prognosis (Travis et al. 2000). On HRCT, NSIP is characterized by patchy ground-glass opacities combined with irregular linear or reticular opacities and scattered micronodules (Johkoh et al. 2002) (Fig. 26.5a,b). In advanced disease, fibrotic changes, such as microcystic honeycombing and traction bronchiectasis, become more evident (Desai et al. 2004). In contrast to the heterogeneous lung involvement and the typical apicobasal gradient in UIP, HRCT in NSIP reveals rather symmetric and homogeneous lung involvement without an obvious gradient (Fig. 26.6).

26.3.1.3 Cryptogenic Organizing Pneumonia

COP was formerly referred to as *bronchiolitis obliterans organizing pneumonia (BOOP)* and is characterized by the histologic pattern of organizing pneumonia (OP). There is no gender predilection. Patients usually present between 50 and 60 years of age, and typically report

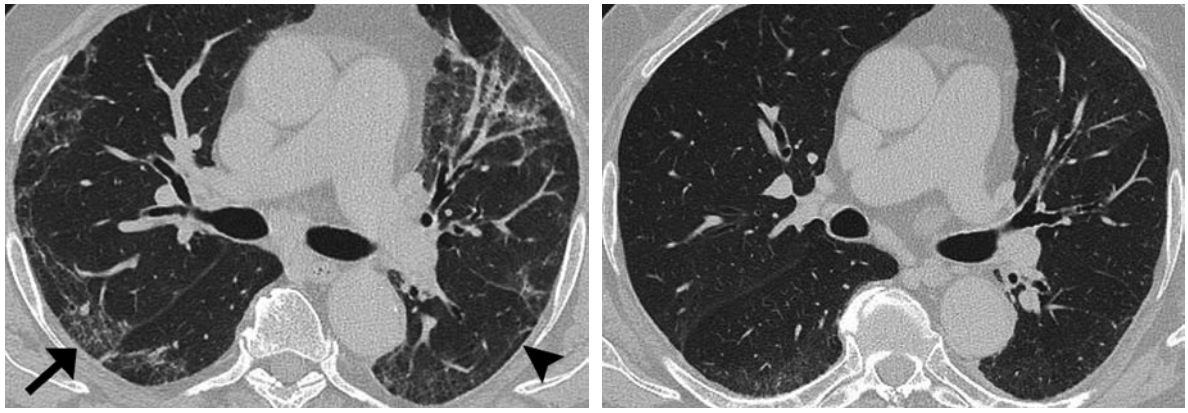

Fig. 26.5a,b. Axial CT image in a 61-year-old man with NSIP shows bilateral subpleural irregular linear opacities (*arrowhead*) and ground-glass opacities (*arrow*) (**a**). Follow-up CT image obtained after 6 months of corticosteroid therapy shows improvement, with partial resolution of the linear opacities and ground-glass opacities (**b**)

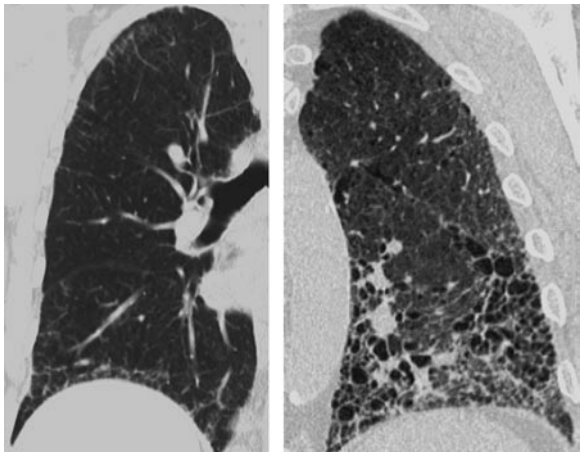

Fig. 26.6. Comparison of CT features between NSIP and UIP. NSIP (*left*) shows diffuse lung involvement with bilateral, peripherally located linear and reticular opacities. In UIP (*right*), the lung abnormalities show a typical apicobasal gradient with predominance of honeycombing

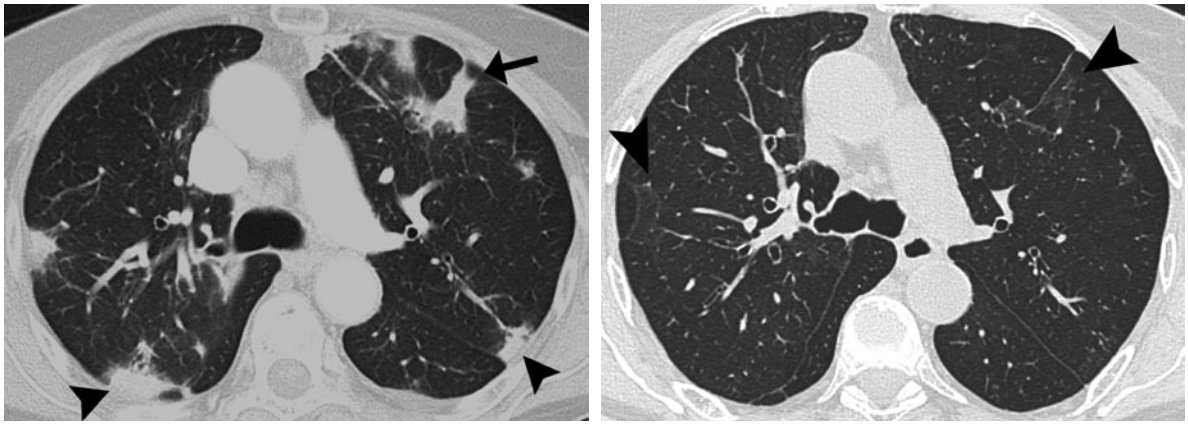

Fig. 26.7a,b. Axial CT image in a 75-year-old woman with COP shows bilateral, peripherally located patchy lung consolidation (*arrowheads*) In one of the lesions, the subpleural space is typically spared (*arrow*) (**a**). Follow-up CT image obtained after 4 weeks of corticosteroid therapy shows subtotal resolution of the lung abnormalities with residual ground-glass opacities (*arrowheads*) (**b**)

a respiratory tract infection preceding their symptoms. In its idiopathic form (as COP), OP is rare; however, it is frequently encountered in association with collagen vascular diseases, and in infectious and drug-induced lung diseases (Cordier 2000). On corticosteroid therapy, patient usually experience complete recovery, but relapses are common. The histologic hallmark of COP is the development of granulation tissue polyps within the alveolar ducts and alveoli, with preservation of the lung architecture. On HRCT, COP is characterized by patchy peripheral or peribronchial consolidations that resemble pneumonic infiltrates and predominate in the lower lung lobes (Lee et al. 1994) (Fig. 26.7a,b). Frequently, air bronchograms and perifocal ground-glass opacities can be found. Other common findings include sparing of the outermost subpleural area and mild cylindrical bronchiectasis. In addition to these typical CT features, other less specific findings can be encountered, such as irregular linear opacities, solitary focal lesions, and multiple nodules (Akira et al. 1998), and diagnosis should be confirmed with surgical lung biopsy.

26.3.1.4 Respiratory Bronchiolitis-Associated Interstitial Lung Disease

RB-ILD is exclusively encountered in smokers and is thought to represent a symptomatic variant of the histologically common and incidental finding of respiratory bronchiolitis (RB). Patients are usually 30–50 years old, and men are affected nearly twice as often as are women. After smoking cessation, prognosis is excellent. Histologically, RB-ILD is characterized by pigmented alveolar macrophages within the bronchioles. The typical HRCT features of RB-ILD are centrilobular nodules ("airspace nodules," small nodules with ground-glass opacity) that are randomly distributed or have upper lobe predominance (Heyneman et al. 1999) (Fig. 26.8). Additional CT features are diffuse ground-glass opacities, bronchial wall thickening, and co-existing centrilobular emphysema (Fig. 26.9).

26.3.1.5 Desquamative Interstitial Pneumonia

DIP is strongly associated with cigarette smoking and is considered to represent the end of a spectrum of RB-ILD. There is a male predominance, and patients usually present between 30 and 50 years of age. Most patients improve with smoking cessation and corticosteroid therapy. Histologically, DIP shows diffuse involvement, with filling of alveolar spaces with macrophages and desquamated alveolar cells, compared to the bronchiolocentric involvement in RB-ILD. On HRCT, DIP is characterized by extensive and diffuse ground-glass opacities with peripheral and lower lobe predominance (Akira et al. 1997) (Fig. 26.10). The presence of small cystic spaces and irregular linear opacities is indicative of fibrotic changes.

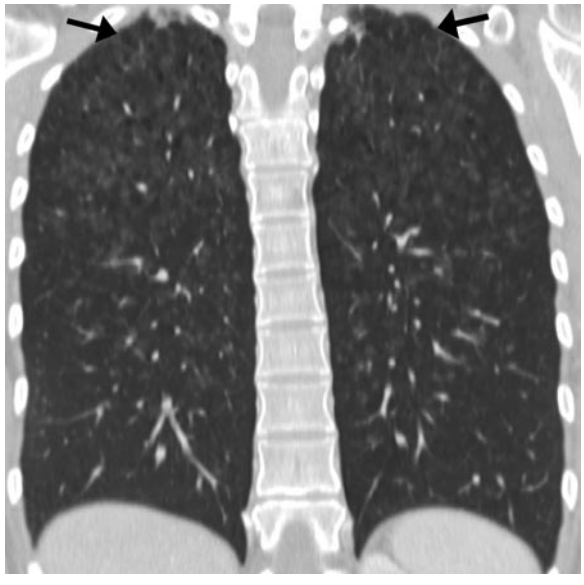

Fig. 26.8. RB-ILD in a 44-year-old female cigarette smoker. Coronal CT image shows scattered, poorly defined centrilobular nodules that are predominantly located in the upper lung lobes. Note mild coexisting centrilobular emphysema (*arrows*)

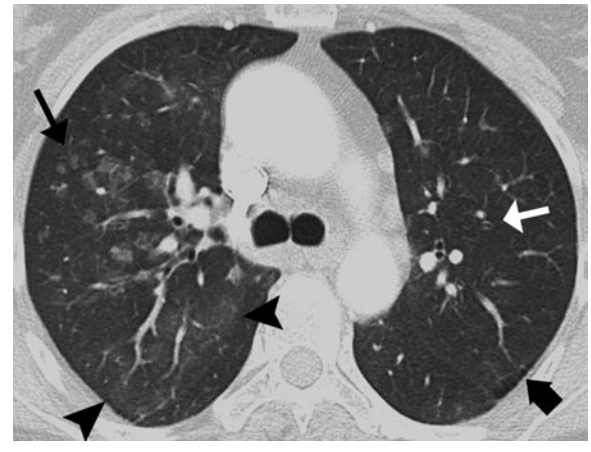

Fig. 26.9. RB-ILD. Axial CT image shows centrilobular nodules (*thin black arrow*), patchy ground-glass opacities (*arrowheads*), and mild bronchial wall thickening (*white arrow*). Note discrete paraseptal emphysema (*thick black arrow*)

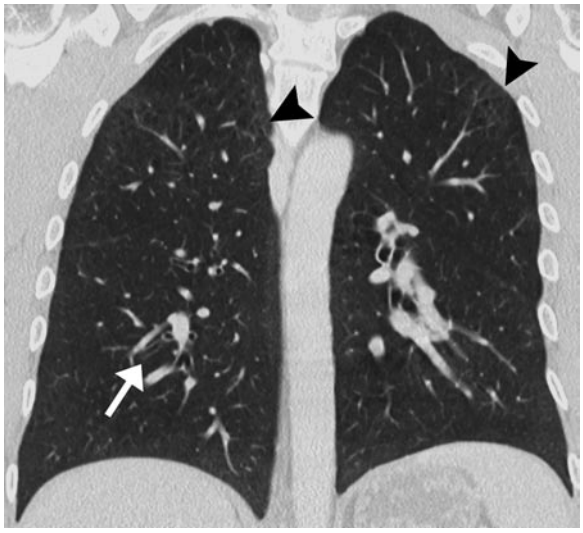

Fig. 26.10. Desquamative interstitial pneumonia (DIP). Coronal CT image shows bilateral, peripheral ground-glass opacities and coexisting moderate bronchial wall thickening (*arrow*). In some areas, small cystic spaces are present (*arrowheads*)

26.3.1.6 Lymphoid Interstitial Pneumonia

LIP rarely occurs as an idiopathic disease. It is usually seen in conjunction with systemic disorders, most notably human immunodeficiency virus (HIV) infection, Sjögren's syndrome, and variable immunodeficiency syndromes (Swigris et al. 2002). LIP is more common in women than in men, and typically, patients become symptomatic in the fifth decade of life. Histologically, LIP is characterized by diffuse interstitial cellular infiltrates that are composed of lymphocytes, plasma cells, and histiocytes. While the interstitium is expanded by these infiltrates, the alveolar airspaces are partially collapsed. The HRCT findings of LIP consist of bilateral, diffuse, or patchy ground-glass opacities, poorly defined centrilobular nodules, and cystic air spaces (Fig. 26.11). The mechanism of cyst formation has been postulated to be secondary to partial bronchiolar obstruction with air trapping due to peribronchiolar lymphocytic infiltration (Desai et al. 1997).

26.3.1.7 Acute Interstitial Pneumonia

AIP differs from the other IIPs in its acute course of disease, with rapid onset of dyspnea and cough, which is followed by respiratory failure and a high acute mortality rate of 50% or more (the American Thoracic Society and the European Respiratory Society 2002). AIP was formerly referred to as *Hamman-Rich syndrome*. The histological and radiological features of AIP are similar to those of acute respiratory distress syndrome (ARDS) and can be subdivided into an acute or exudative phase and a late or organizing phase. CT obtained in the early phase shows extensive ground-glass opacities, sometimes in a geographic distribution (Fig. 26.12a). In addition, areas of consolidation can be observed in the dependent areas of the lungs. In pa-

Fig. 26.11. Lymphoid interstitial pneumonia (LIP) in a 48-year-old woman. Axial CT image shows extensive ground-glass opacities and scattered thin-walled cysts

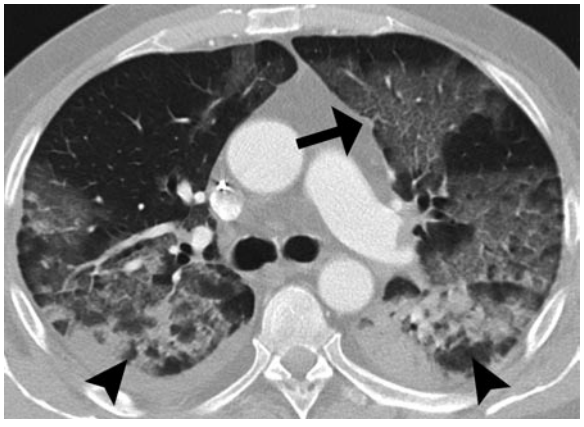

a

Fig. 26.12a,b. Acute interstitial pneumonia (AIP) in a 58-year-old patient. **a** Axial CT image shows bilateral ground-glass opacities in a geographic distribution (*arrow*). Consolidation is seen in the more dependent lung (*arrowheads*). Small, coexisting bilateral pleural effusions are present. **b** (*see next page*)

Fig. 26.12a,b. (*continued*) Acute interstitial pneumonia (AIP) in a 58-year-old patient. **b** Fibrotic changes with traction bronchiectasis (*arrow*) and architectural distortion in the late phase of acute interstitial pneumonia (AIP)

tients who survive the acute phase of disease, CT shows fibrotic changes with architectural distortion and traction bronchiectasis, predominantly in the nondependent areas of the lung (Fig. 26.12b).

26.3.2 Sarcoidosis

Sarcoidosis is a common systemic disorder of unknown cause characterized by the presence of noncaseating granulomas, which either can dissolve or cause fibrosis. Almost any organ can be affected, but the lungs are most frequently involved.

The mean age of patients is between 20 and 40 years, and there is a slight female predominance (Costabel and Hunninghake 1999). In up to 50% of patients, sarcoidosis is incidentally discovered on radiographs. Common clinical symptoms include respiratory illness, skin lesions, fatigue, and weight loss. Lofgren's syndrome is a classic clinical presentation with fever, erythema nodosum, arthralgias, bihilar lymphadenopathy, and a usually benign course of disease.

The diagnosis is established on the basis of clinical and radiological findings, supported by histology from transbronchial biopsy. Spontaneous remissions occur in nearly two-thirds of patients, but the course is chronic or progressive in 10–30% (Costabel and Hunninghake 1999). The appropriate treatment depends on clinical and imaging findings and is based on corticosteroids. In patients with end-stage sarcoidosis, lung transplantation has been successfully performed, but is associated with high recurrence rates of sarcoidosis (35%) (Collins et al. 2001).

For the staging of sarcoidosis, a system based on chest radiographs is in clinical use; stage I consists of bilateral hilar adenopathy; in stage II sarcoidosis, patients have bilateral hilar adenopathy and diffuse parenchymal infiltration; stage III describes parenchymal infiltration without hilar adenopathy. Some authorities use a stage IV classification to indicate irreversible fibrosis.

In patients with sarcoidosis, CT scans of the lung are now included routinely in the diagnostic workup at initial evaluation and at follow-up. Specifically, they are indicated in the setting of atypical clinical and/or chest radiograph findings, for the detection of complications of the lung disease (e.g., pulmonary fibrosis, superimposed infection, malignancy), and when chest radiographs are normal, despite clinical suspicion of the disease (Costabel and Hunninghake 1999). For these indications, the combination of the classic HRCT and a sequential MDCT protocol should be used.

The chest can be involved in sarcoidosis in many ways, and because of the multitude of potentially different findings, sarcoidosis can be regarded as one of the "great mimickers" in thoracic radiology. The most common intrathoracic manifestation of sarcoidosis is the presence of mediastinal lymphadenopathy with usually bilateral and rather symmetric involvement of hilar lymph nodes. They can calcify in chronic disease

Fig. 26.13. A 27-year-old woman with chronic sarcoidosis. Coronal CT image displays extensive mediastinal lymphadenopathy. Lymph nodes show punctuate calcifications

and then show amorphous, punctate, or eggshell calcifications (Fig. 26.13). In patients with sarcoidosis and parenchymal involvement, nodular opacities are the predominant finding. These nodules typically range in size between 1 and 5 mm and are often ill defined. They have a perilymphatic distribution, and thus preferentially lie adjacent to the fissures, along pleural surfaces, and along central vascular structures (Fig. 26.14). There is a predilection for the upper lobes and the superior segments of the lower lobes of both lungs.

Sarcoid nodules sometimes tend to coalesce and form large parenchymal nodules with surrounding loosely aggregated small nodules. As the shape of these coalescent granulomas resembles a galaxy, it is referred to as the "sarcoid galaxy sign" (Nakatsu et al. 2002) (Fig. 26.15). Occasionally, a single, large nodule may be present in sarcoidosis and resemble bronchogenic carcinoma. Ground-glass opacities are common in sarcoidosis and have been postulated to represent alveolitis in early reports; however, according to pathologic correlation, ground-glass opacities in sarcoidosis are more likely to represent microgranulomas with or without perigranulomatous fibrosis (Nishimura et al. 1993). Patients with predominant ground-glass opacities on initial CT scan have a worse prognosis than have patients with a predominant nodular pattern (Murdoch and Muller 1992; Akira et al. 2005).

When sarcoidosis progresses to fibrosis, architectural distortion and traction bronchiectasis classically radiating from the hilum to the adjacent upper and lower lobes can be found. Other common CT abnormalities in fibrotic sarcoidosis include honeycombing, cysts, and bulla formation. Airway stenosis in sarcoidosis is usually due to extrinsic scarring, or to endobronchial granulomas, whereas lymphadenopathy alone is a rare cause of symptomatic airway narrowing.

Pneumoconiosis may simulate the appearance of sarcoidosis, but is usually easily diagnosed when correlated with clinical history. Primary tuberculosis, lymphoma, and mediastinal metastases from other tumors usually present with asymmetrical nodal enlargement as opposed to the bihilar, and often-symmetric hilar lymphadenopathy in stage I sarcoidosis.

Fig. 26.14a,b. A 31-year-old woman with sarcoidosis. **a** Axial CT image shows multiple uniformly sized nodules as well as nodular thickening of the interlobar septa and the bronchial walls. **b** The upper lobe predominance of the nodules can be seen on the coronal CT image

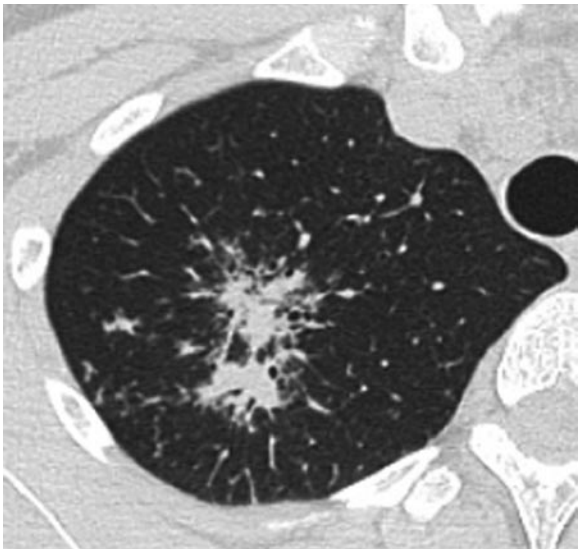

Fig. 26.15. A 41-year-old man with sarcoidosis. The parenchymal nodules in the right upper lobe tend to coalesce and form a large parenchymal nodule surrounded by loosely aggregated small nodules. As this resembles a galaxy, it is referred to as the "sarcoid galaxy sign"

26.3.3 Miscellaneous Rare Forms of Interstitial Lung Disease of Unknown Etiology

26.3.3.1 Pulmonary Langerhans Cell Histiocytosis

Pulmonary Langerhans cell histiocytosis (PLCH) (formerly called *histiocytosis X*) is a rare interstitial lung disease of unknown cause that primarily affects cigarette smokers under 40 years of age. Most patients present with cough and dyspnea; sometimes additional systemic symptoms, such as fatigue, weight loss, and fever, are reported. Smoking cessation is the most important component in the therapeutic management of PLCH, with stabilization or regression of clinical and radiographic features in the majority of patients. CT is very sensitive for the detection of PLCH, and a correct diagnosis can be achieved in over 80% of cases (Grenier et al. 1991). On CT, PLCH is characterized by a combination of small nodules (1–10 mm) and cysts. The cysts are thought to arise by cavitation of the nodules, have a variable wall thickness, and are often irregularly outlined (Abbott et al. 2004) (Fig. 26.16a). Usually, the lung abnormalities are most prominent in the upper lobes, with relative sparing of the lung bases near the costophrenic sulci (Fig. 26.16b). In later phases of the disease, nodules are less obvious, and cysts are the predominant feature. In this setting, PLCH may mimic lymphangioleiomyomatosis, but the latter occurs almost exclusively in women, affects the lung diffusively without sparing of the lung bases, and is characterized by uniformly sized cysts.

26.3.3.2 Lymphangioleiomyomatosis

Lymphangioleiomyomatosis (LAM) is a rare interstitial lung disease that affects women of childbearing age exclusively. The tuberous sclerosis complex (TSC), an autosomal dominant inherited disorder, is associated with parenchymal lung changes identical to LAM (Pallisa et al. 2002).

Histologically, LAM is characterized by an abnormal proliferation of smooth muscle cells (LAM cells) in the lungs and in the thoracic and retroperitoneal lymphatics. The most common initial presenting symptoms are dyspnea, spontaneous pneumothorax, and cough (Johnson 1999). The clinical course of LAM is variable. Normally, the disease progresses slowly, with continuous deterioration of pulmonary function. Ultimately, it leads to respiratory failure. Because LAM deteriorates with pregnancy and the use of exogenous estrogen, several attempts at anti-estrogen therapies have been made, with controversial results (Taylor et al. 1990). Lung transplantation is indicated in patients with end-stage disease. Apart from the common postoperative complications of transplantation, recurrent disease in the donor lung can occur.

The key findings on CT are uniformly distributed, thin-walled cysts that tend to conflate (Fig. 26.17). The cysts can be up to 3 cm in diameter and are equally and symmetrically distributed throughout both lungs. Usu-

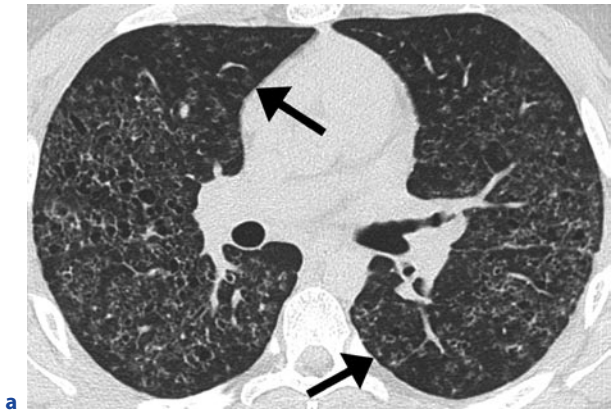

a

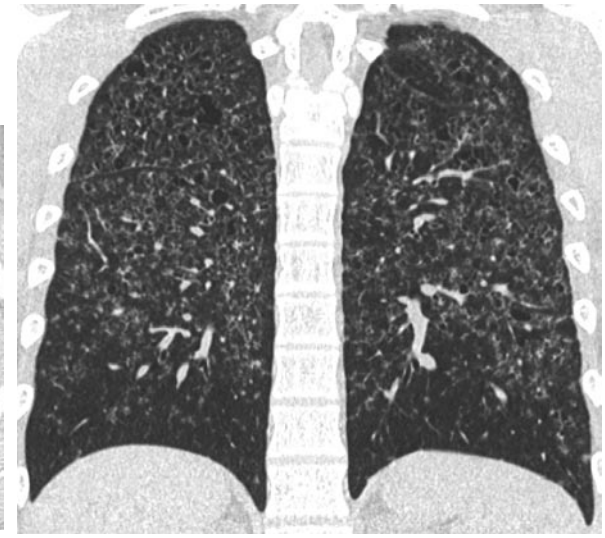

b

Fig. 26.16a,b. Pulmonary Langerhans cell histiocytosis in a 26-year-old man. **a** Axial CT image demonstrates bilateral, thin-walled cysts of variable size and multiple, ill-defined nodules (*arrows*). **b** Coronal CT image better demonstrates the upper and middle lung zone predominance, with relative sparing of the lung bases

Fig. 26.17a,b. A 30-year-old woman with tuberous sclerosis complex. **a** Axial CT image shows multiple thin-walled cysts in a uniform distribution. The cysts adjacent to the upper right mediastinum tend to conflate (*white arrows*). **b** Coronal CT image displays the uniform and bilateral distribution of the cysts throughout both lungs. The lung parenchyma between the cysts is inconspicuous

ally, the cyst shape is round; however, in some cases, they can be of ovoid, polygonal, or irregular shape. Cyst wall thickness ranges from barely susceptible to up to 2 mm. On expiratory scans, cyst size decreases, suggesting a communication with the airway system. The lung parenchyma in between the cysts is usually inconspicuous, but, in the highly cellular forms of LAM, small nodules, reticular opacification, and ground-glass attenuation can be found (Aberle et al. 1990). Pneumothorax is common in LAM, and occurs in about 80% of patients within the course of the disease. About 8–14% of patients develop pulmonary hemorrhage, which presents as ground-glass opacity on HRCT (Lenoir et al. 1990). Pleural chylous effusions can be found in up to 14% of patients, and are indistinguishable from protein-rich effusions of other origin on CT. In addition, dilatation of the thoracic duct, as well as mediastinal, hilar, and retrocrural adenopathy, can be found in patients with LAM.

In more than 70% of patients with LAM, renal angiomyolipomas can be found, which show a characteristic appearance, with negative CT values due to their fat content. In some cases, retroperitoneal cystic hypoattenuating masses indicative of lymphangioleiomyomas can be found. Chylous ascites and lymphadenopathy are further extrathoracic findings in some patients (Pallisa et al. 2002).

The most important differential diagnoses for LAM are Langerhans cell histiocytosis, idiopathic pulmonary fibrosis, and panlobular emphysema. In contrast to LAM, in Langerhans cell histiocytosis, the costophrenic sulci are usually spared, the cysts can be thick-walled and irregularly outlined, and nodules are predominant in the early stage of disease. Idiopathic pulmonary fibrosis shows a volume loss in contrast to LAM, and the honeycomb cysts are predominantly located in the lower lobes and subpleural (Bonelli et al. 1998). Panlobular emphysema is associated with alpha-1-antiprotease deficiency. The most distinct feature of emphysema is the absence of defined walls in the areas of low attenuation, whereas cysts in LAM almost invariably present with walls (Johnson 1999).

26.3.3.3 Eosinophilic Pneumonia

Eosinophilic pneumonia is divided into acute eosinophilic pneumonia (AEP) and chronic eosinophilic pneumonia (CEP). The pathogenesis of both forms is still unknown, but it is speculated to be a hypersensitivity reaction to an unknown antigen. However, AEP has been reported after cigarette smoking, dust exposure, and smoke from fireworks. The mean age of patients with CEP is 40; AEP occurs at all ages. AEP shows no gender predominance, whereas CEP occurs more often in women. Histologically, diffuse alveolar damage associated with interstitial and alveolar eosinophilia is found in AEP (Tazelaar et al. 1997); in CEP, an accumulation of eosinophils and lymphocytes in the interstitium and alveoli, and sometimes, interstitial fibrosis, is found.

AEP clinically presents as an acute febrile illness with dyspnea, pleuritic chest pain, myalgias, and respiratory failure. In AEP, blood eosinophilia is often absent, but more than 25% eosinophils are found in the bronchial lavage fluid of these patients. CEP has an insidious onset with fever, malaise, weight loss, and dyspnea. About 90% of these patients suffer from asthmatic symp-

toms. In CEP, peripheral blood eosinophilia is present in more than 90% of cases, and there are an increased number of eosinophils in the bronchial lavage fluid as well (Allen and Davis 1994). Both AEP and CEP are often misdiagnosed as pneumonia, which can delay the correct diagnosis for months. Both AEP and CEP show a rapid response to corticosteroids, and there usually is rapid clearing of clinical and radiographic abnormalities within several days (Allen and Davis 1994).

At CT, AEP shows bilateral peripheral ground-glass opacities, with lower-lobe predominance (Fig. 26.18). In addition, interlobar septal thickening and thickening of the bronchovascular bundles, as well as localized areas of consolidation, can be seen. AEP is very commonly associated with pleural effusions, and band-like opacities paralleling the chest wall are nearly pathognomonic (Allen and Davis 1994; Johkoh et al. 2000).

CEP shows upper lobe predominance and peripheral nonsegmental consolidations (Fig. 26.19). Consolidations can persist for some time, but, in the absence of treatment, they tend to migrate. Consolidations are often accompanied by ground-glass opacities, and a "crazy paving" appearance of the consolidations can also be appreciated in many cases. Pleural effusions are rare in CEP (Mayo et al. 1989; Johkoh et al. 2000).

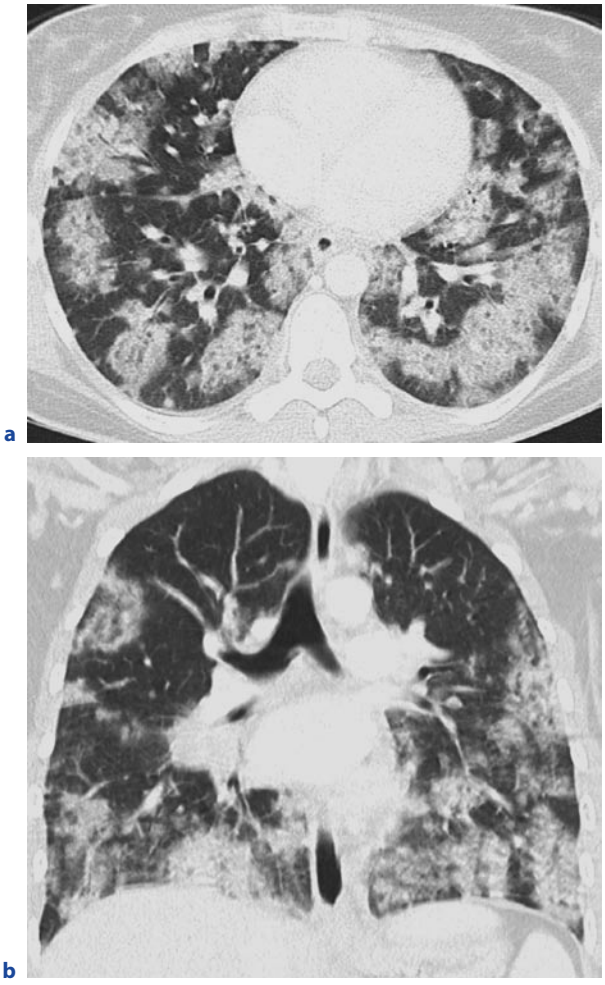

Fig. 26.18a,b. Acute eosinophilic pneumonia in a 37-year-old female with BAL fluid eosinophilia. **a** Axial CT image obtained 5 days after onset of dyspnea shows peripherally distributed patchy areas of consolidation and ground-glass opacities accompanied by interlobular septal thickening. **b** Coronal CT image displays the lower lobe predominance of the infiltrates

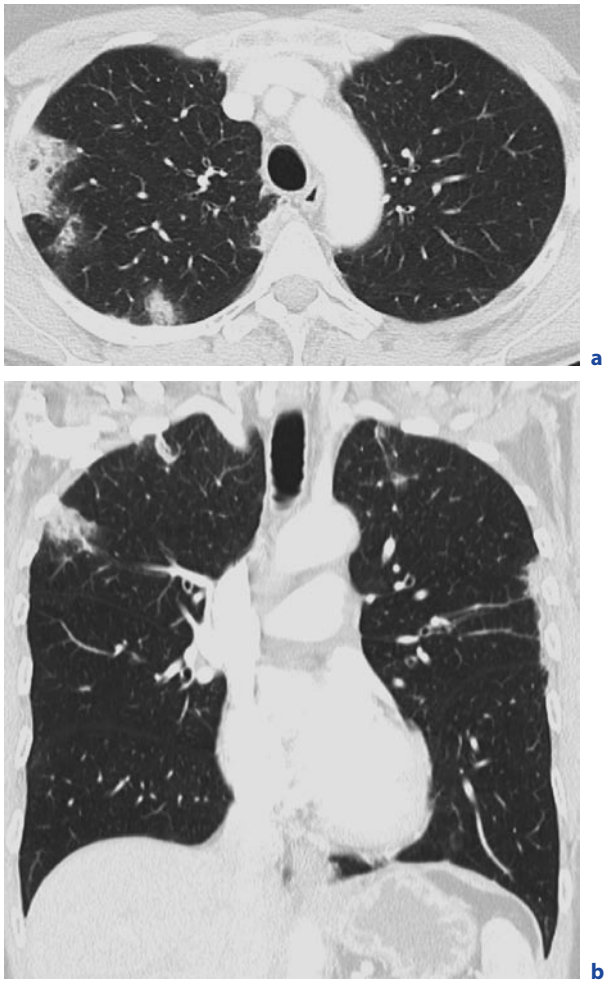

Fig. 26.19a,b. Chronic eosinophilic pneumonia in a 56-year-old man presenting with a 4-week history of cough and fever. Moderate blood eosinophilia is found in laboratory workup. **a** Axial CT image shows strikingly peripheral wedge-shaped airspace consolidations. **b** The upper lobe predominance of the consolidations is displayed on coronal CT image

The differential diagnoses include simple pulmonary eosinophilia (Löffler's syndrome), Churg–Strauss syndrome, cryptogenic organizing pneumonia (COP), pulmonary infarcts, aspiration pneumonia, and diffuse pulmonary hemorrhage. In Löffler's syndrome, patients are usually asymptomatic, and opacities are rather fleeting. Churg–Strauss syndrome is usually accompanied by a systemic disease, which is not present in CEP or AEP. In contrast to CEP, cryptogenic organizing pneumonia has lower lobe predominance, but the infiltrates can be similar to CEP. Pulmonary infarcts are more wedge-shaped than are infiltrates seen in CEP or AEP. Aspiration pneumonia is found in gravity-dependent lung regions and is commonly associated with small airways disease. Diffuse pulmonary hemorrhage presents with diffuse pulmonary consolidations, but these consolidations usually have a diffuse pattern, and a history of renal disease, anemia, and hemoptysis is common in such cases (Mayo et al. 1989; Allen and Davis 1994; Johkoh et al. 2000).

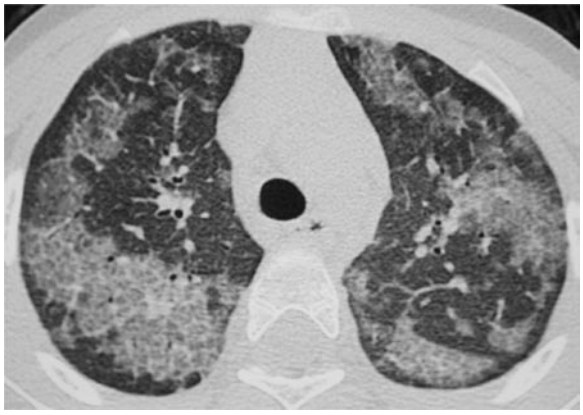

Fig. 26.20. Alveolar proteinosis in 40-year-old man with myelogenous leukemia presenting with cough and dyspnea. Axial CT image displays bilateral geographical areas of ground-glass opacity. Interlobular septa are thickened and within these areas, a fine reticular network of interlobular lines can be seen. These changes are referred to as the typical "crazy-paving" appearance of alveolar proteinosis

26.3.3.4 Pulmonary Alveolar Proteinosis

Pulmonary alveolar proteinosis (PAP) is a rare interstitial lung disease, characterized by filling of the alveoli with a lipid-rich proteinaceous material (Rosen et al. 1958). Three different forms of PAP can be distinguished: an autosomal recessive congenital form (2%); a secondary form (10%) that is associated with various conditions, such as hematopoietic disorders (especially myelogenous leukemias), silicosis, immunodeficiency disorders, malignancies, and some infections; and an idiopathic form (90%). In idiopathic PAP, several mechanisms are responsible for phospholipid accumulation in the alveoli. Whether this accumulation is caused by reduced clearance or overproduction is not yet clear (Prakash et al. 1987). The median age of the patients is about 40 years, and most patients are men and have a history of smoking (Ben-Dov et al. 1999). Patients present with dyspnea or cough. The symptoms are usually out of proportion to the radiological findings (clinical–radiological discrepancy). In 13% of patients with PAP, secondary infections with nocardia, cryptococci, or mycobacteria are observed. The treatment for PAP is bronchoalveolar lavage with sterile saline, and prognosis is generally good with whole-lung lavage.

HRCT is characterized by bilateral, symmetrical, geometric areas of ground-glass attenuation (Fig. 26.20). The interlobular septa are thickened, and a fine network of interlobular lines can be seen. These changes are responsible for the so-called "crazy-paving" pattern. The disease does not have any preferential zonal distribution (Holbert et al. 2001). Architectural distortion and bronchiectasis are absent normally; however, in a small percentage of patients, pulmonary fibrosis can be found. Although the crazy-paving pattern on HRCT is suggestive of PAP, this pattern can also be observed in a number of other interstitial and air-space diseases, such as pulmonary hemorrhage, pulmonary edema, hypersensitivity pneumonitis, and alveolar cell carcinoma. The diagnosis can be made by bronchoalveolar lavage and typical clinical findings. Nevertheless, the gold standard in diagnosis remains open lung biopsy.

26.3.3.5 Pulmonary Microlithiasis

Pulmonary alveolar microlithiasis (PAM) is a rare condition characterized by the formation of intra-alveolar microliths (calcospherites). The pathogenesis of the micronodular calcifications is still unknown. In about 50% of cases, pulmonary alveolar microlithiasis occurs as an autosomal recessive hereditary lung disease (Sosman et al. 1957). Most cases of microlithiasis are found in Turkey (Ucan et al. 1993). The disease usually occurs between 30 and 50 years of age, and pediatric cases are rare. In hereditary cases, there is slight female predominance.

The disease is typically detected incidentally on chest films obtained for other reasons, and clinical symptoms are disproportional to the extent of radiologic findings. Occasionally, patients present with stress-induced dyspnea, malaise, or fatigue. As PAM progresses with the formation of tiny (0.01–3mm) microspheres in the alveoli, it can ultimately lead to respiratory failure and cor pulmonale.

In early stages, diffuse ground-glass opacifications are found throughout both lungs on CT. Still, the presence of calcified micronodules is most characteristic. The distribution of the micronodules is miliary, but there is a tendency toward greater involvement of the posterior segments of the lower lobes and the anterior segments of the upper lobes (Fig. 26.21). Due to the intra and periseptal accumulation of micronodules, interlobular septal thickening is found in almost all patients. In addition, subpleural septal thickening is frequently detected.

As the disease progresses, subpleural emphysema and the formation of thin-walled subpleural cysts are pathognomonic findings in PAM and might represent early lung fibrosis. The subpleural cysts are accountable for the black subpleural line on chest X-rays (Korn et al. 1992). The main differential diagnoses include miliary tuberculosis, sarcoidosis, metastatic pulmonary calcification associated with hemodialysis, silicosis, and pulmonary hemosiderosis.

Usually, the disease progresses very slowly, but can result in cardiac and pulmonary failure. There is no known treatment, except lung transplantation in end-stage disease.

26.4 Interstitial Lung Diseases of Known Cause

26.4.1 Occupational and Environmental Lung Disease

Occupational and environmental lung disease comprises a wide spectrum of lung disorders caused by the inhalation or ingestion of organic and inorganic particles and chemicals. CT is very sensitive in depicting the parenchymal, as well as airway and pleural abnormalities that are associated with these diseases.

26.4.1.1 Hypersensitivity Pneumonitis

Hypersensitivity pneumonitis (HP), also known as *exogenous allergic alveolitis* (*EEA*), is an immunologic lung disease caused by repeated exposure and sensitization to various organic and chemical antigens, which leads to diffuse inflammation of the lung parenchyma. The most common diseases are farmer's lung and bird fancier's lung due to *Aspergillus* antigens and avian proteins, respectively. Based on the length and intensity of exposure and subsequent duration of illness, clinical presentations of HP are categorized as acute, subacute, and chronic progressive. In acute HP, patients present 4–12 h after heavy exposure to an inciting agent with

Fig. 26.21. A 37-year-old man with pulmonary alveolar microlithiasis. Axial CT image shows miliary distributed calcified micronodules predominantly located in the middle and lower zones of both lungs. Also note the formation of small subpleural cysts and subpleural emphysema and the formation of the pathognomonic black subpleural line (*white arrows*)

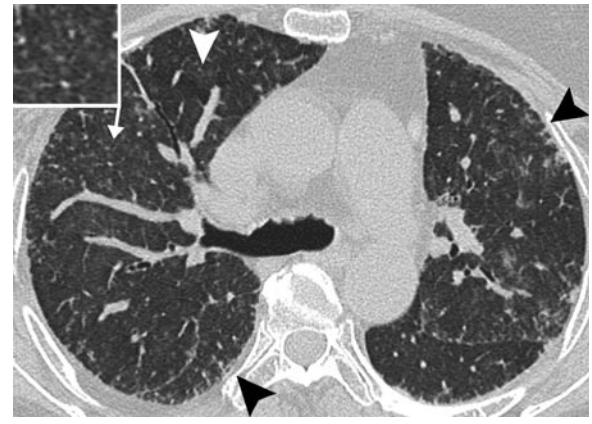

Fig. 26.22. Chronic hypersensitivity pneumonitis in a 52-year-old man, related to mold exposure. Axial CT image shows patchy ground-glass opacities with associated centrilobular nodules (*inset* magnified view of centrilobular nodules). Also note mild subpleural reticular opacities (*black arrowheads*) indicating fibrosis, and subtle mosaic attenuation (*white arrowhead*)

fever, chills, and myalgias. In subacute and chronic HP, patients have an insidious onset of cough, progressive dyspnea, fatigue, and weight loss. CT in acute HP typically shows diffuse ground-glass opacities and centrilobular nodules, most commonly in a random distribution (Tomiyama et al. 2000). In the subacute phase, centrilobular nodules become more prominent, and patchy ground-glass opacities can be found. In some patients, cystic lesions (3–25mm) have been observed (Franquet et al. 2003). Chronic HP is characterized by the presence of reticulation due to fibrosis superimposed on findings of subacute HP (Fig. 26.22). The abnormalities are usually predominantly located in the upper lobes, while the lung bases are relatively spared (Silva et al. 2008). Other common findings in chronic HP include a mosaic attenuation pattern and air trapping on expiratory imaging (Small et al. 1996).

26.4.1.2 Pneumoconiosis

Pneumoconiosis is a non-neoplastic reaction to the inhalation and accumulation of dust particles in the lung.

Fig. 26.23. Silicosis with progressive massive fibrosis in a 72-year-old man. Coronal CT image shows a large mass in the right medial upper lobe (*arrowhead*). There is retraction of the hilus and marked emphysema. In addition, some scattered small nodules are present

The particles are engulfed by alveolar macrophages that release inflammatory cytokines and induce fibrotic changes. The classification of pneumoconiosis is based on chest radiographs using the International Labor Organization (ILO) classification scheme. The CT features in patients with silicosis and coal worker pneumoconiosis consist of small, well-circumscribed nodules that are usually 2–5mm in diameter and predominantly affect the upper and posterior lung zones. The nodules in silicosis tend to be larger and better defined than those nodules in coal worker pneumoconiosis (Kim et al. 2001). Occasionally, eggshell calcifications in the hilar and mediastinal lymph nodes are seen. The presence of nodules larger than 1 cm is indicative of complicated pneumoconiosis, also known as *progressive massive fibrosis*. These nodules coalesce and form conglomerate masses that are typically located in the upper lobe of the lung. In large lesions, cavitation may occur, which is due to either ischemic necrosis or superinfection. In advanced disease, hilar retraction and compensatory emphysema, particularly in the lower lobes, is seen (Fig. 26.23).

The parenchymal lung manifestations related to asbestos exposure are referred to as *asbestosis* and differ from the previously described "classic" pneumoconiosis. Early asbestosis is characterized by subpleural linear and reticular opacities that are predominantly located in the posterior lung bases. To distinguish these abnormalities from gravity-related physiologic changes, prone scans should be included in cases of suspected asbestosis. Other typical findings in asbestosis include thickened interlobular septa and centrilobular nodules. In advanced disease, CT shows bands of fibrosis, traction bronchiectasis, and honeycombing. In addition, other asbestos-related lung abnormalities, such as pleural effusion, pleural plaques, and round atelectasis can be found.

26.4.1.3 Drug-Induced Lung Injury

Drug-induced lung injury is a common cause of acute and chronic lung disease, and most commonly occurs with cytotoxic agents, such as bleomycin, busulfan, carmustine, and cyclophosphamide (Ellis et al. 2000). Chemotherapeutic drugs can result in four main types of lung reaction: interstitial pneumonia (IP), diffuse alveolar damage (DAD)/ARDS, organizing pneumonia (OP) (formerly referred to as BOOP), and hypersensitivity reaction. The CT manifestations of IP are identical to the pattern of NSIP, and consist of scattered ground-glass opacities and irregular linear opacities

(Fig. 26.24). In early drug-induced DAD (first week after lung injury), CT shows diffuse ground-glass opacities and consolidations, whereas, in the late phase of disease (after 1 or 2 weeks), fibrotic changes occur, such as irregular linear opacities, architectural distortion, and traction bronchiectasis. Drug-induced OP is identical to COP, and manifests on CT with bilateral areas of ground-glass opacities or consolidations that are often peripheral in distribution. Hypersensitivity reactions usually become clinically apparent within hours or days after institution of drug therapy, and patients typically present with progressive dyspnea, cough, fever, and peripheral eosinophilia (Rossi et al. 2000). Pulmonary involvement can result in either acute or chronic EP. CT in EP shows ground-glass opacities and consolidation that are typically distributed peripherally and in the upper lobe. EP usually responds well to cessation of the administered drug and is exceedingly sensitive to corticosteroid therapy. Within the group of noncytotoxic drugs, methotrexate and amiodarone frequently cause drug-induced lung diseases in 5–10% of patients. The most common lung injury associated with both drugs is interstitial pneumonia. Organizing pneumonia is less commonly associated with noncytotoxic drugs (Fig. 26.25).

26.4.2 Radiation-Induced Lung Injury

Radiation-induced lung injury is subdivided clinically and radiologically into an early stage, characterized by acute radiation pneumonitis, and a late stage, characterized by chronic radiation fibrosis. The degree of radiation damage to normal tissue depends particularly on total dose and the fraction of that dose, irradiated volume, individual susceptibility, preexisting lung disease, and previous or concomitant therapy. Early radiation pneumonitis usually develops 1 to 3 months after the therapy, and the radiographic findings are typically confined to the field of radiation, resulting in a geometric shape of pulmonary opacities with a sharp demarcation line at noninvolved lung areas and disregard of anatomic boundaries. The earliest CT findings consist of subtle ground-glass opacities (Fig. 26.26). These hazy abnormalities can progress to patchy consolidations that sometimes also involve lung areas outside the field of radiation (Davis et al. 1992). Chronic radiation fibrosis evolves within 6 to 24 months after radiation therapy and develops continuously from the phase of acute pneumonitis. At CT, it is characterized by the presence of reticular opacities, architectural distortion, traction bronchiectasis, and volume loss. The major differential diagnoses in radiation pneumonitis include infection, lymphangitic carcinomatosis, and recurrence of the original malignancy. Microbial infectious pneumonia is not usually confined to the field of irradiation and runs a clinical course more symptomatic than the course of radiation pneumonitis. In lymphangitic carcinomatosis, the rapid worsening of radiographic abnormalities, with development of irregular, often-nodular thickening of

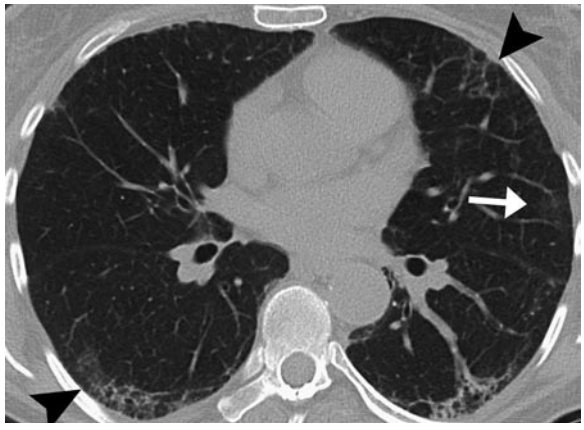

Fig. 26.24. A 50-year-old woman with interstitial pneumonia (IP)/nonspecific interstitial pneumonia (NSIP) after bleomycin chemotherapy for Hodgkin's lymphoma. Axial CT image shows irregular linear and reticular opacities (*arrowheads*) with subtle ground-glass opacities (*arrow*) in subpleural distribution

Fig. 26.25. A 63-year-old man with organizing pneumonia (OP). The patient was receiving amiodarone for cardiac arrhythmia. Coronal CT image shows bilateral areas of ground-glass opacities in subpleural distribution (*arrowheads*)

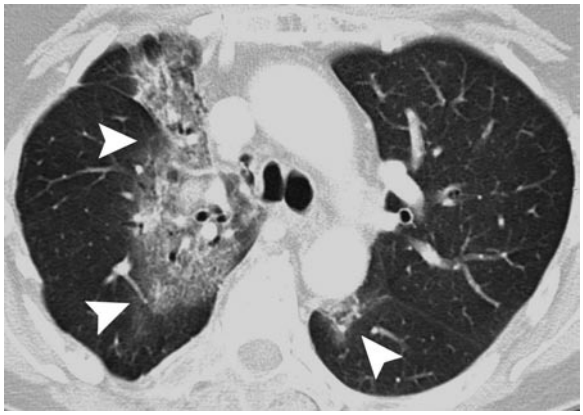

Fig. 26.26. Acute radiation pneumonitis after treatment of lung cancer. Axial CT image obtained at 4 months after completion of treatment shows paramediastinal ground-glass opacities with sharp lateral margins (*arrowheads*)

the interlobular septa and the bronchovascular bundles, pleural effusions, and diffuse spread to the lung, are the diagnostic clues. In patients with suspected radiation therapy, it is advisable to utilize a volumetric CT protocol in order to avoid missing focal disease representing tumor recurrence or metastases.

26.4.3 Collagen Vascular Lung Disease

Lung involvement is common in patients with collagen vascular diseases and may be detected with CT before the disease has declared itself or been accurately characterized. Interstitial lung disease is probably most prevalent in systemic sclerosis, but is also a common problem in rheumatoid arthritis (RA), mixed connective tissue disease, dermatomyositis/polymyositis (DMPM), or Sjögren's syndrome. Lung involvement less frequently occurs with systemic lupus erythematosus (SLE). The parenchymal manifestations of collagen vascular diseases seen at CT closely resemble those found in IIPs and can be classified using the same system. Although the proportions of interstitial pneumonias vary, the NSIP is the most frequently encountered pattern in patients with collagen vascular lung disease, especially in progressive systemic sclerosis (Fig. 26.27). In keeping with the IIPs, the NSIP pattern is characterized by subpleural reticular opacities and varying proportions of ground-glass opacities, while in patients with UIP, honeycombing and traction bronchiectasis are the dominant abnormality. The predominance of the NSIP over the UIP pattern might explain the more favorable prognosis in patients with interstitial pneumonia associated with collagen vascular diseases than in those with IIPs (Kim et al. 2002). OP is more common in RA than in the other collagen vascular diseases and is characterized by patchy infiltrates in a peripheral distribution. LIP is a typical, but rare complication in Sjögren's syndrome in about 1% of patients during the course of their disease (Swigris et al. 2002), and CT findings include diffuse or patchy ground-glass opacities and thin-walled perivascular cysts (Fig. 26.28). In addition to the patterns of interstitial pneumonias, other parenchymal manifestations in collagen vascular diseases include al-

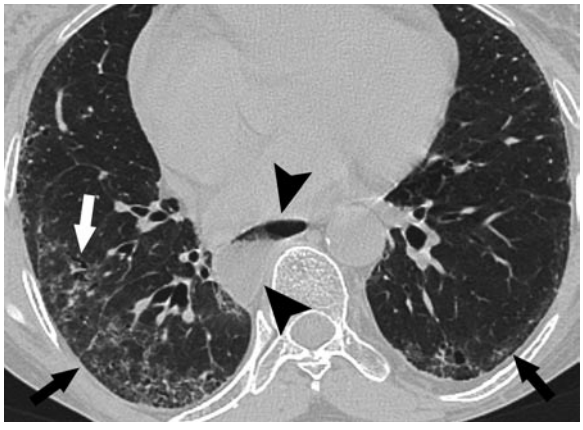

Fig. 26.27. Axial CT image in a patient with progressive systemic sclerosis shows a mixture of fine reticular and ground-glass opacities (*black arrows*), associated with mild traction bronchiectasis (*white arrow*), consistent with a nonspecific interstitial pneumonia pattern. Note esophageal dilatation (*arrowheads*)

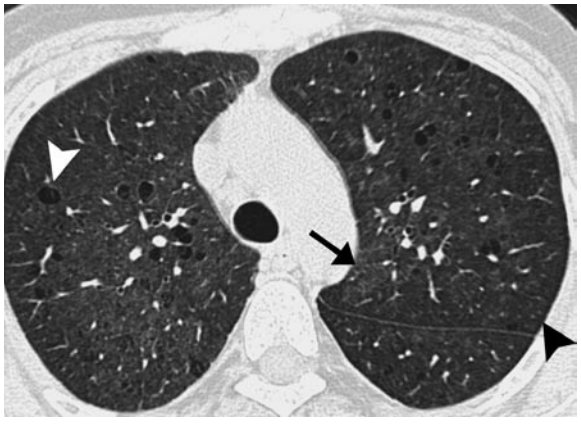

Fig. 26.28. LIP in a 44-year-old woman with Sjögren's syndrome. Axial CT image shows several thin-walled cysts (*white arrowhead*), bilateral patchy ground-glass opacities (*arrow*), and poorly defined centrilobular nodules (*black arrowhead*)

veolar hemorrhage, especially in patients with SLE, and necrobiotic nodules in patients with RA, which range in size from a few millimeters to a few centimeters (Remy-Jardin et al. 1994), and are usually subpleural in distribution. The increased prevalence of malignant disorders complicating the course of some disorders such DMPM makes volumetric CT protocols mandatory in the follow-up of these patients.

26.4.4 Diffuse Pulmonary Hemorrhage

Diffuse bleeding into the alveolar spaces most commonly occurs with immunological and hematological disorders and is clinically characterized by hemoptysis and anemia (Albelda et al. 1985); however, the absence of these symptoms does not rule out the diagnosis of diffuse pulmonary hemorrhage (DPH). DPH must be distinguished from localized pulmonary hemorrhage due to chronic bronchitis, bronchiectasis, tumor, and infection. DPH can occur in association with many collagen vascular diseases, notably SLE and Wegener's granulomatosis. Other rare causes of DPH include Goodpasture's syndrome and idiopathic pulmonary hemosiderosis. CT is more sensitive than is chest radiograph for the detection of pulmonary hemorrhage, and shows diffuse bilateral consolidation or ground-glass opacities in the acute phase (Marasco et al. 1993). In the subacute phase of DPH, multiple small nodules associated with patchy ground-glass opacities and interlobular septal thickening have been observed (Fig. 26.29). In addition, in patients with Wegener's granulomatosis, multiple, frequently cavitating nodules and masses, ranging from 5 mm to 10 cm, can be seen.

Fig. 26.29. Goodpasture's syndrome in a 21-year-old-man. CT scan shows multiple nodules, subtle ground-glass opacities (*arrow*), and mild interlobular thickening (*arrowhead*)

References

Abbott GF, Rosado-de-Christenson ML et al. (2004) From the archives of the AFIP: pulmonary Langerhans cell histiocytosis. Radiographics 24:821–841

Aberle DR, Hansell DM et al. (1990) Lymphangiomyomatosis: CT, chest radiographic, and functional correlations. Radiology 176:381–387

Akira M, Kozuka T et al. (2005) Long-term follow-up CT scan evaluation in patients with pulmonary sarcoidosis. Chest 127:185–191

Akira M, Yamamoto S et al. (1997) Serial computed tomographic evaluation in desquamative interstitial pneumonia. Thorax 52:333–337

Akira M, Yamamoto S et al. (1998) Bronchiolitis obliterans organizing pneumonia manifesting as multiple large nodules or masses. AJR Am J Roentgenol 170:291–295

Albelda SM, Gefter WB et al. (1985) Diffuse pulmonary hemorrhage: a review and classification. Radiology 154:289–297

Allen JN, Davis WB (1994) Eosinophilic lung diseases. Am J Respir Crit Care Med 150:1423–1438

Anonymous (1999) Statement on sarcoidosis. Joint Statement of the American Thoracic Society (ATS), the European Respiratory Society (ERS) and the World Association of Sarcoidosis and Other Granulomatous Disorders (WASOG) adopted by the ATS Board of Directors and by the ERS Executive Committee, February 1999. Am J Respir Crit Care Med 160:736–755

Anonymous (2002) American Thoracic Society/European Respiratory Society International Multidisciplinary Consensus Classification of the Idiopathic Interstitial Pneumonias. This joint statement of the American Thoracic Society (ATS), and the European Respiratory Society (ERS) was adopted by the ATS board of directors, June 2001 and by the ERS Executive Committee, June 2001. Am J Respir Crit Care Med 165:277–304

Ben-Dov I, Kishinevski Y et al. (1999) Pulmonary alveolar proteinosis in Israel: ethnic clustering. Isr Med Assoc J 1:75–78

Bonelli FS, Hartman TE et al. (1998) Accuracy of high-resolution CT in diagnosing lung diseases. AJR Am J Roentgenol 170:1507–1512

Bouros D, Hatzakis K et al. (2002) Association of malignancy with diseases causing interstitial pulmonary changes. Chest 121:1278–1289

Collins J, Hartman MJ et al. (2001) Frequency and CT findings of recurrent disease after lung transplantation. Radiology 219:503–509

Cordier JF (2000) Organising pneumonia. Thorax 55:318–328

Costabel U, Hunninghake GW (1999) ATS/ERS/WASOG statement on sarcoidosis. Sarcoidosis Statement Committee. American Thoracic Society. European Respiratory Society. World Association for Sarcoidosis and Other Granulomatous Disorders. Eur Respir J 14:735–737

Davis SD, Yankelevitz DF et al. (1992) Radiation effects on the lung: clinical features, pathology, and imaging findings. AJR Am J Roentgenol 159:1157–1164

Desai SR, Nicholson AG et al. (1997) Benign pulmonary lymphocytic infiltration and amyloidosis: computed tomographic and pathologic features in three cases. J Thorac Imaging 12:215–220

Desai SR, Veeraraghavan S et al. (2004) CT features of lung disease in patients with systemic sclerosis: comparison with idiopathic pulmonary fibrosis and nonspecific interstitial pneumonia. Radiology 232:560–567

Ellis SJ, Cleverley JR et al. (2000) Drug-induced lung disease: high-resolution CT findings. AJR Am J Roentgenol 175:1019–1024

Franquet T, Hansell DM et al. (2003) Lung cysts in subacute hypersensitivity pneumonitis. J Comput Assist Tomogr 27:475–478

Grenier P, Valeyre D et al. (1991) Chronic diffuse interstitial lung disease: diagnostic value of chest radiography and high-resolution CT. Radiology 179:123–132

Hansell DM (2001) High-resolution CT of diffuse lung disease: value and limitations. Radiol Clin North Am 39:1091–1113

Heyneman LE, Ward S et al. (1999) Respiratory bronchiolitis, respiratory bronchiolitis-associated interstitial lung disease, and desquamative interstitial pneumonia: different entities or part of the spectrum of the same disease process? AJR Am J Roentgenol 173:1617–1622

Holbert JM, Costello P et al. (2001) CT features of pulmonary alveolar proteinosis. AJR Am J Roentgenol 176:1287–1294

Johkoh T, Muller NL et al. (2000) Eosinophilic lung diseases: diagnostic accuracy of thin-section CT in 111 patients. Radiology 216:773–780

Johkoh T, Muller NL et al. (2002) Nonspecific interstitial pneumonia: correlation between thin-section CT findings and pathologic subgroups in 55 patients. Radiology 225:199–204

Johnson S (1999) Rare diseases. 1. Lymphangioleiomyomatosis: clinical features, management and basic mechanisms. Thorax 54:254–264

Katzenstein AL, Myers JL (1998) Idiopathic pulmonary fibrosis: clinical relevance of pathologic classification. Am J Respir Crit Care Med 157:1301–1315

Kim DS, Park JH et al. (2006) Acute exacerbation of idiopathic pulmonary fibrosis: frequency and clinical features. Eur Respir J 27:143–150

Kim EA, Lee KS et al. (2002) Interstitial lung diseases associated with collagen vascular diseases: radiologic and histopathologic findings. Radiographics 22:S151–S165

Kim KI, Kim CW et al. (2001) Imaging of occupational lung disease. Radiographics 21:1371–1391

Korn MA, Schurawitzki H et al. (1992) Pulmonary alveolar microlithiasis: findings on high-resolution CT. AJR Am J Roentgenol 158:981–982

Lee KS, Kullnig P et al. (1994) Cryptogenic organizing pneumonia: CT findings in 43 patients. AJR Am J Roentgenol 162:543–546

Lenoir S, Grenier P et al. (1990) Pulmonary lymphangiomyomatosis and tuberous sclerosis: comparison of radiographic and thin-section CT findings. Radiology 175:329–334

Marasco WJ, Fishman EK et al. (1993) Acute pulmonary hemorrhage. CT evaluation. Clin Imaging 17:77–80

Mayo JR, Webb WR et al. (1987) High-resolution CT of the lungs: an optimal approach. Radiology 163:507–510

Mayo JR, Muller NL et al. (1989) Chronic eosinophilic pneumonia: CT findings in six cases. AJR Am J Roentgenol 153:727–730

Mueller-Mang C, Grosse C et al. (2007) What every radiologist should know about idiopathic interstitial pneumonias. Radiographics 27:595–615

Murata K, Itoh H et al. (1986) Centrilobular lesions of the lung: demonstration by high-resolution CT and pathologic correlation. Radiology 161:641–645

Murdoch J, Muller NL (1992) Pulmonary sarcoidosis: changes on follow-up CT examination. AJR Am J Roentgenol 159:473–477

Nakatsu M, Hatabu H et al. (2002) Large coalescent parenchymal nodules in pulmonary sarcoidosis: sarcoid galaxy sign. AJR Am J Roentgenol 178:1389–1393

Nishimura K, Itoh H et al. (1993) Pulmonary sarcoidosis: correlation of CT and histopathologic findings. Radiology 189:105–109

Pallisa E, Sanz P et al. (2002) Lymphangioleiomyomatosis: pulmonary and abdominal findings with pathologic correlation. Radiographics 22:S185–S198

Prakash UB, Barham SS et al. (1987) Pulmonary alveolar phospholipoproteinosis: experience with 34 cases and a review. Mayo Clin Proc 62:499–518

Remy-Jardin M, Remy J et al. (1994) Lung changes in rheumatoid arthritis: CT findings. Radiology 193:375–382

Rosen SH, Castleman B et al. (1958) Pulmonary alveolar proteinosis. N Engl J Med 258:1123–1142

Rossi SE, Erasmus JJ et al. (2000) Pulmonary drug toxicity: radiologic and pathologic manifestations. Radiographics 20:1245–1259

Silva CI, Muller NL et al. (2008) Chronic hypersensitivity pneumonitis: differentiation from idiopathic pulmonary fibrosis and nonspecific interstitial pneumonia by using thin-section CT. Radiology 246:288–297

Small JH, Flower CD et al. (1996) Air-trapping in extrinsic allergic alveolitis on computed tomography. Clin Radiol 51:684–688

Sosman MC, Dodd GD et al. (1957) The familial occurrence of pulmonary alveolar microlithiasis. Am J Roentgenol Radium Ther Nucl Med 77:947–1012

Studler U, Gluecker T et al. (2005) Image quality from high-resolution CT of the lung: comparison of axial scans and of sections reconstructed from volumetric data acquired using MDCT. AJR Am J Roentgenol 185:602–607

Swigris JJ, Berry GJ et al. (2002) Lymphoid interstitial pneumonia: a narrative review. Chest 122:2150–2164

Taylor JR, Ryu J et al. (1990) Lymphangioleiomyomatosis. Clinical course in 32 patients. N Engl J Med 323:1254–1260

Tazelaar HD, Linz LJ et al. (1997) Acute eosinophilic pneumonia: histopathologic findings in nine patients. Am J Respir Crit Care Med 155:296–302

Thabut G, Mal H et al. (2003) Survival benefit of lung transplantation for patients with idiopathic pulmonary fibrosis. J Thorac Cardiovasc Surg 126:469–475

Tomiyama N, Muller NL et al. (2000) Acute parenchymal lung disease in immunocompetent patients: diagnostic accuracy of high-resolution CT. AJR Am J Roentgenol 174:1745–1750

Travis WD, Matsui K et al. (2000) Idiopathic nonspecific interstitial pneumonia: prognostic significance of cellular and fibrosing patterns: survival comparison with usual interstitial pneumonia and desquamative interstitial pneumonia. Am J Surg Pathol 24:19–33

Ucan ES, Keyf AI et al. (1993) Pulmonary alveolar microlithiasis: review of Turkish reports. Thorax 48:171–173

Webb WR (2006) Thin-section CT of the secondary pulmonary lobule: anatomy and the image—the 2004 Fleischner lecture. Radiology 239:322–338

Weibel ER (1979) Fleischner lecture. Looking into the lung: what can it tell us? AJR Am J Roentgenol 133:1021–1031